227005

Computational Instability arising from YIN-YANG Boundary

Masami SAKAMOTO[1], Kohei KAWANO[1] , Kohei ARANAMI[1], Tabito HARA[1], Hiroshi KUSABIRAKI[1], Junichi ISHIDA[1], Chiashi MUROI[1], and Yuji KITAMURA[2]

[1]Numerical Prediction Division, Forecast Department, Japan Meteorological Agency (NPD/JMA) [2]Forecast Laboratory, Meteorological Research Institute (MRI)

1. Introduction

Yin-Yang Grid is a composite mesh proposed by Kageyama and Sato (2004). This technique allows us to create a global numerical weather prediction (NWP) model using a regional dynamical core.

In 2009, Japan Meteorological Agency (JMA) initiated a fundamental research to develop a global non-hydrostatic NWP model, and a Yin-Yang Grid model, which is planned to use a regional model ASUCA (Ishida et al. 2010), has been one of candidates for a further development.

In the course of developing shallow-water models and a three-dimensional model, we have encountered computational instability problems. We have analyzed results to overcome the issues, and found that some of the problems are related to discretization methods and advection schemes.

2. A non-hydrostatic dynamical core "ASUCA"

ASUCA is a regional NWP model developed by JMA, which

• adopts the finite volume method (FVM) using the flux limiter proposed by Koren (1993), which allows us the monotonicity and conservation of scalar predictor variables without using artificial numerical diffusion / viscosity,

• offers capability to accommodate some map projections, using the general coordinate transformations, including

➢ the Lambert conformal conic projection for regional forecasts

➢ the Spherical curvilinear coordinates (latitude-longitude projection) necessary for the yin-yang expansion,

• uses the 3rd order Runge - Kutta time integration scheme proposed in Hundsdorfer et al. (1995).

In this study, a yin-yang grid composition using features above is examined.

2.1 flux limiter by Koren(1993)

Total flux used in the finite volume method using Arakawa-C grid is

$\partial p_i/\partial t = (F_{i-1/2} - F_{i+1/2}) / \Delta x$,

where p_i is a predictor at i^{th} grid, $F_{i-1/2}$ and $F_{i+1/2}$ are flux of p at both end of the grid, and Δx is size of the grid. Flux limiter "b" is used to estimate flux,

$F_{i+1/2} = u_{i+1/2} [p_i + b_{i+1/2} (p_{i+1} - p_i) /2]$, $F_{i-1/2} = u_{i-1/2} [p_{i-1} + b_{i-1/2} (p_i - p_{i-1})/2]$.

where $u_{i+1/2}$ and $u_{i-1/2}$ are flow speed at both end. Koren (1993) definded his limiter "b" as

$b_{i+1/2} = \max[0, \min(2r_i, (r_i + 2)/3, 2)]$, $b_{i-1/2} = \max[0, \min(2r_{i-1}, (r_{i-1} + 2)/3, 2)]$.

where $r_i = (p_i - p_{i-1})/(p_{i+1} - p_i)$, and $r_{i-1}=(p_{i-1} - p_{i-2})/(p_i - p_{i-1})$.

When r is large enough (means steep gradient of p), estimated flux approaches to the 1st order upwind scheme:

$F_{i+1/2} = \{u_{i+1/2} (p_i + p_{i+1}) + |u_{i+1/2}| (p_i - p_{i+1}) \}/2$,
$F_{i-1/2} = \{u_{i-1/2} (p_{i-1} + p_i) + |u_{i-1/2}| (p_{i-1} - p_i) \}/2$.

Advection tests for scalar signals

• 360 grids with the periodic boundary condition at the edges are used to calculate advection; $\partial h/\partial t = \nabla(uh)$. The grid intervals and the time steps are the same ($\Delta x = 1$, $\Delta t = 1$).

• Hundsdorfer et al. (1995) is used as a time integration method.

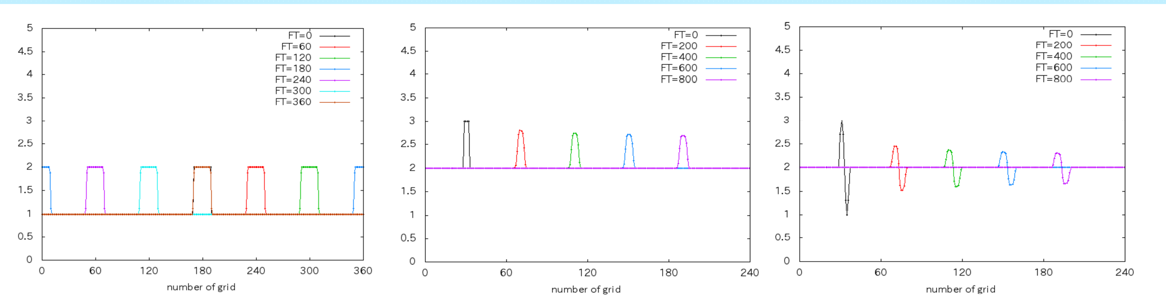

[Left Panel] uses 20Δx length of a rectangular signal, and propagation velocity c=1 (therefore courant number is: cΔt/Δx=1). [Center Panel] Velocity c=0.2 (courant number :cΔt/Δx=0.2) with 4Δx length rectangular signal. [Right Panel] Velocity c=0.2 and an 8Δx length sine curve shaped signal.

Power spectrum density for zonal / meridional wind speed, and potential temperature at Level-13 (near 850hPa) from regional forecasts for east Japan

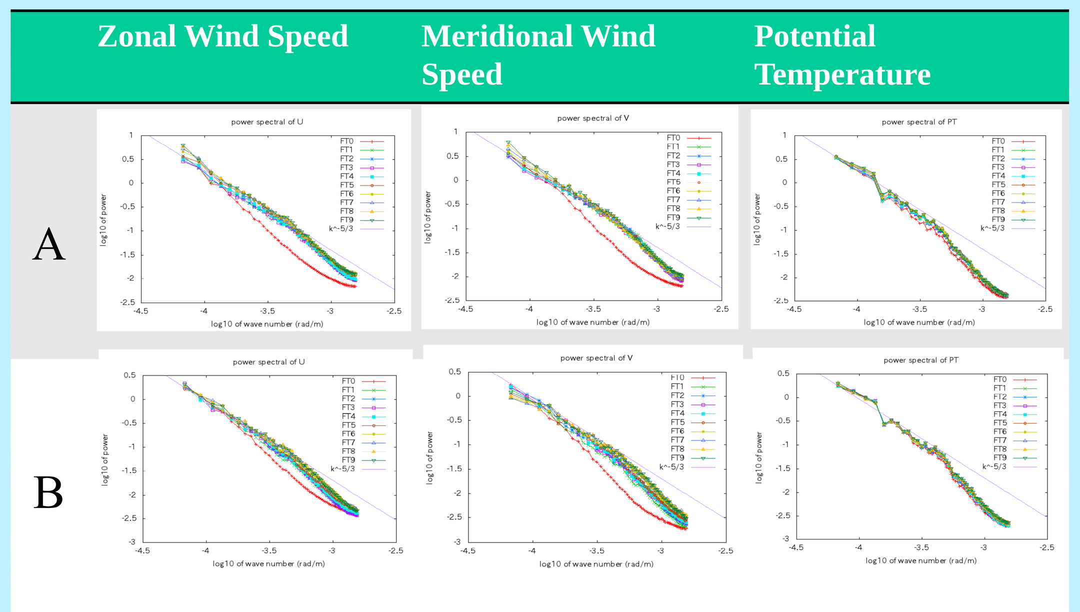

A: 8 forecasts during 19 – 25, July, 2011, B: 7 forecasts during 24 – 30, August, 2011

2.2 Runge-kutta 3rd scheme by Hundsdorfer et al. (1995)

Runge-kutta 3rd Method by Hundsdorfer et al. (1995),

$p^* = p^t + (\partial p^t/\partial t) \Delta t/3$
$p^{**} = p^t + (\partial p^*/\partial t) \Delta t/2$
$p^{t+\Delta t} = p^t + (\partial p^{**}/\partial t) \Delta t$

General Runge-kutta 3rd Method,

$p^* = p^t + (\partial p^t/\partial t)\Delta t/2$
$p^{**} = p^t + (\partial p^*/\partial t) 2\Delta t - (\partial p^t/\partial t) \Delta t$
$p^{t+\Delta t} = p^t + (\partial p^t/\partial t + 4 \partial p^*/\partial t + \partial p^{**}/\partial t) \Delta t/6$

Runge-kutta 4th Method,

$p^* = p^t + (\partial p^t/\partial t)\Delta t/2$
$p^{**} = p^t + (\partial p^*/\partial t)\Delta t/2$
$p^{***} = p^t + (\partial p^{**}/\partial t)\Delta t$
$p^{t+\Delta t} = p^t+(\partial p^t/\partial t+2\partial p^*/\partial t+2\partial p^{**}/\partial t+\partial p^{***}/\partial t)\Delta t/6$

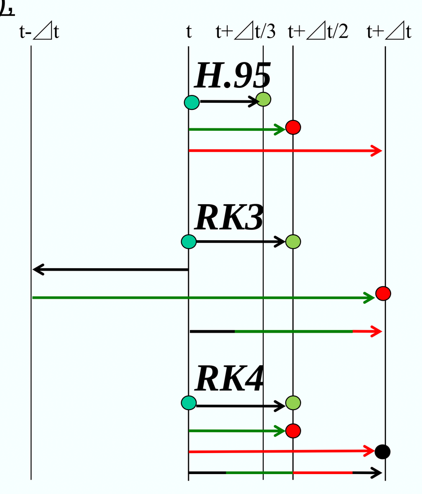

where p^t and $p^{t+\Delta t}$ are scalar values at time t and t+Δt respectively.

Williamson et al. (1992) test cast 1 (advection test)

α=0, Courant number:1.0, after one round

Mass Conservation(L_1): $\int(\rho_{fcst} - \rho_{true})ds / \int\rho_{true} ds$

H.95	RK3	RK4
8.3×10^{-4}	6.3×10^{-4}	5.6×10^{-4}

L_2 norm: $(\int(\rho_{fcst} - \rho_{true})^2 ds / \int\rho_{true}^2 ds)^{1/2}$

H.95	RK3	RK4
3.6×10^{-2}	4.2×10^{-2}	4.4×10^{-2}

L_∞ norm: $\max | \rho_{fcst} - \rho_{true}| / \max |\rho_{true} |$

H.95	RK3	RK4
4.8×10^{-2}	5.8×10^{-2}	6.4×10^{-2}

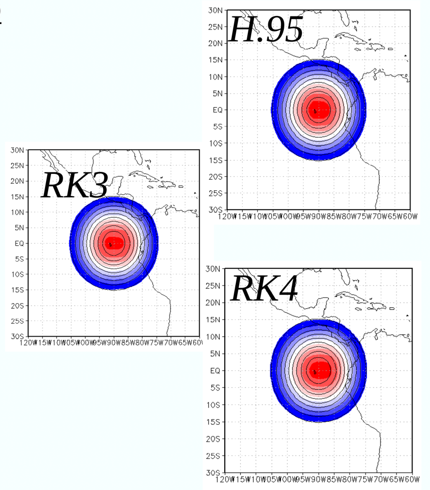

3. Problems found and analyzed in this study

We discuss two issues below;

A) Flux adjustment schemes like Peng et al. (2006) can cause errors, and may develop computational instability when adopting the finite volume method. To avoid the issue, a flux adjustment techniques at the boundary can be kind of a nonholonomic system and should be abandoned.

B) There might be a possibility that a tiny discrepancy within the overlapped area for the boundary region exchange method (Sugimura et al. 2006) arises substantial errors, and results in computational instabilities. To moderate the issue, modification in flux estimation and a filter like Shapiro (1971) are effective.

3.A) Influence by a flux adjustment at the boundary

Conservative Constraint by Peng et al. (2006)

(i) Specify the intersections on the boundary referring to both grids.
(ii) Calculate distance between intersections.
(iii) Calculate overlapped areas using trapezoidal rule.
(iv) If the intersection has a grid edge (like H), specify its location referring the other coordinate. Then calculate distances from both ends (E, F).
(v) Compute fluxes (like g_{AB}, g_{BC}, g_{CD}, and g_{AD}) in both systems.
(vi) Calculate the flux along the boundary (EF), using an approximation below

$$\frac{g_{AB} - g_{EF} - \frac{\overline{DF}}{\overline{CD}} g_{CD} + \frac{\overline{BE}}{\overline{BC}} g_{BC} - g_{AD}}{S_{ABEFD}} = \frac{g_{AB} - g_{CD} + g_{BC} - g_{AD}}{S_{ABCD}}$$

$$g_{EF} = \frac{1}{S_{ABCD}} \left\{ (S_{ABEFD} - S_{ABCD}) g_{AB} + \left(\frac{\overline{DF}}{\overline{CD}} S_{ABCD} - S_{ABEFD} \right) g_{CD} + \left(S_{ABEFD} - \frac{\overline{BE}}{\overline{BC}} S_{ABCD} \right) g_{BC} + (S_{ABCD} - S_{ABEFD}) g_{AD} \right\}$$

(vii) Allocate the flux to each segment of the boundary like EH and HF.
(viii) Estimate boundary fluxes using advection in other grid; e. g. $g_{GH} = g_{GE} + g_{EH}$.
(ix) Recalculate advection in boundary grid, substituting boundary fluxes obtained in (viii)

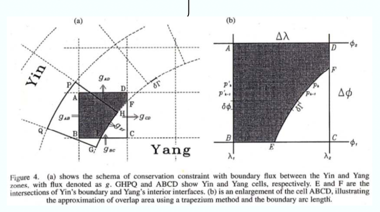

[Figure from Peng et al. (2006)]

Williamson et al. (1992) test case 2 (zonal geostrophic flow)

Thickness of the Fluid: $h^*=h_0 - (a\Omega u_0 + u_0^2/2) (-\cos\lambda \cos\theta \sin\alpha + \sin\theta \cos\alpha)^2$
Speed of the flow: $u = u_0 (\cos\theta \cos\alpha + \sin\theta \cos\lambda \sin\alpha)$, $v = -u_0 \sin\lambda \sin\alpha$
where $u_0 = 2\pi\times a(m/rad)/12(days)/24(hr)/60(min)/60(sec) \fallingdotseq 40$ (m/s) ,
$a = 6.37122 \times 10^6$ (m/rad), $gh_0=2.94 \times 10^4 m^2/s^2$.
h^*: thickness(m), u: zonal speed (m/s), v: meridional speed (m/s) a: radius of the earth (m)
Ω : angular velocity of the earth (rad/s), u_0: maximum flow speed λ: latitude(rad), θ: longitude(rad)
α=0.05(deg) : inclination angle of flow orbit (crock with around the axis through λ=3π/2,θ=0)
Δt = 324sec, $\Delta\theta = \Delta\lambda$ = 2.25deg

Thickness (contour) and its error (shade) after 2day forecast with Conservative Constraint (left), and without it (right)

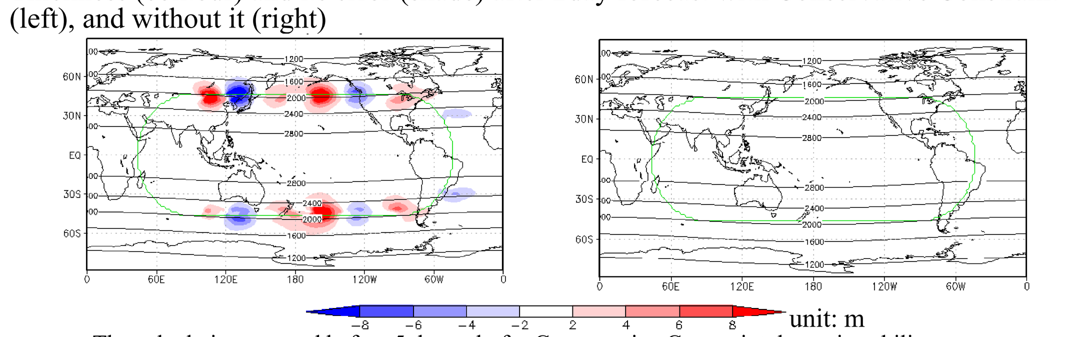

The calculation stopped before 5 day only for Conservative Constraint due to instability
(Note no numerical diffusion / viscosity is used in this test).

One dimensional shallow water test with a cosine bell signal

(180 + 4x2) x2 grids (except for halo regions) for 36,000 m domain is filled with 1m depth of 1kg/m3 fluid, and each grid has 100m length. A cosine bell shaped signal is in the center of the domain at the initial time. Prognostic equations are:

$\partial h/\partial t = \nabla(uh)$, $\partial(uh)/\partial t = \nabla(u^2h) - g h \partial h/\partial x$,

where h is thickness (m), u is velocity (m/s), g is the acceleration of the gravity (m/s^2), t is time (in sec), and Δt=10sec.

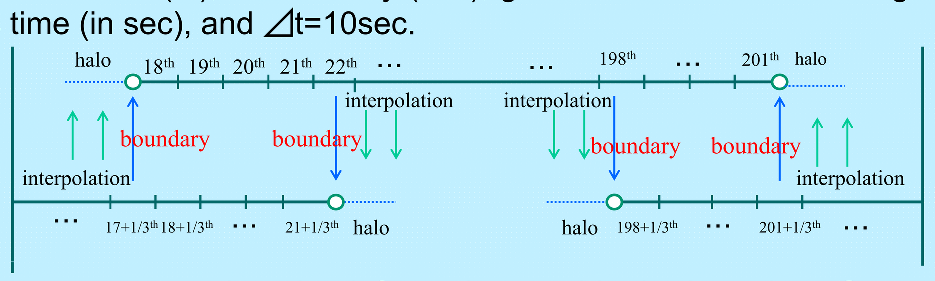

Two grid systems are exchanging information outside the boundary. One starts at 18th position from left end, while another is starting at 198 + 1/3th. When using the boundary (momentum) interpolation, momentum information at boundary points are given from the other side of system. If not, momentum at the boundary positions are calculated by own referring the halo information.

Forecast results of thickness (m) with the boundary momentum exchange (left), without it (center), and with a seamless grid system (right: reference). FT denotes number of time steps integrated.

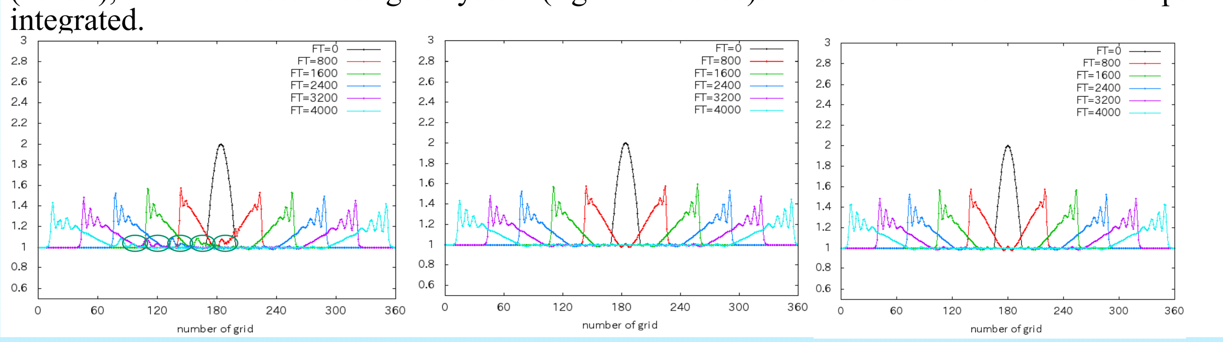

When a boundary momentum adjustment controls momentum at the boundary, the fluid stops and fills up in front of the boundary, and then reflects. The adjustment can be a nonholonomic boundary for FVM. When the same direction of flow continues as seen in case 2 of Williamson et al. (1992), the situation becomes worse, and can result in a computational instability.

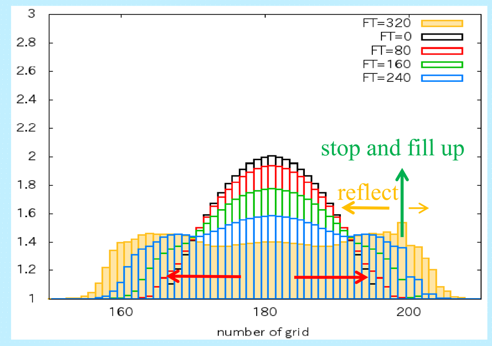

3.B) Discrepancy in the overlapped area may cause problems

Types of Composite Mesh Formation

Boundary Region Exchange (BRE):

The blue grid (yin-grid) receives information at the thick blue region, and the red grid (yang - grid) receives at the thick red area. Forecasts for the overlapped area between the thick areas are calculated in both grids.

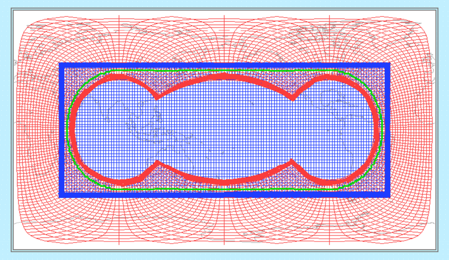

Overlaid Grid Method (OGM):

The both grid calculate and exchange information all over the overlapped area (thick blue and red areas, and the area between them).

Calculation cost and amount of information exchange are larger for OGM than for BRE. OGM requires a data merge procedure, which also needs substantial computational cost. BRE is currently used at JMA (also by Baba et al. 2010). BRE tends to raise high frequency noise, while OGM is inclined to cause distortions in a large scale (Sugihara et al. 2006).

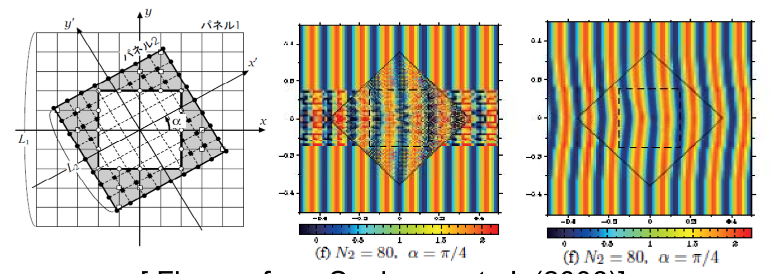

Grid configuration (left), samples of error patterns for BRE (center), and for OGM (right) after Sugihara et al. (2006). The same size of grid panel 1 and 2, inclined 45 degree to each other, calculate advection of sine curve with wavelength 10Δx using advection speed of 12/5 x Δx / Δt and 8.order central finite difference method.

[Figures from Sugimura et al. (2006)]

One dimensional shallow water test with a two-grid length dent

A one dimensional finite volume method model and shallow water prognostic equations, similar to one used in the examination for the boundary momentum interpolation, are adopted. The boundary momentum interpolation is not done, and overlap length are 8+1/3 and 7+2/3 grids instead of 4+1/3 and 3+2/3. As the initial perturbation, a two-grid long dent (left panel below) is given for the upper grid only, while the lower one has no initial perturbation. This is a harsh example of the discrepancy between the upper and lower grids. Δx = 100m, Δt = 10sec, fluid depth = 2m except for the perturbation. The dent depth is 1m.

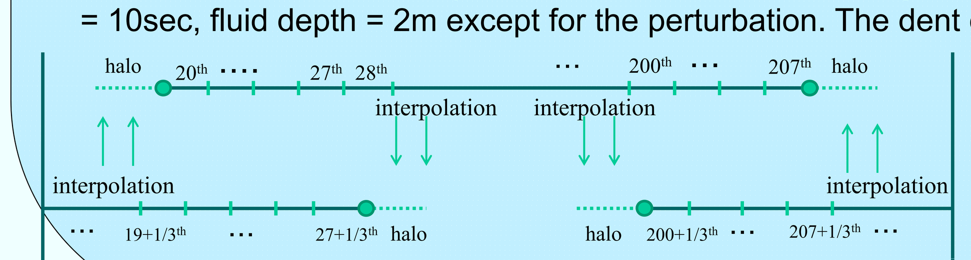

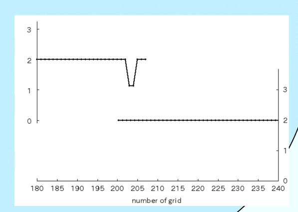

Free surface height referring value from 20 to 199th points of the upper grid, and from 200+1/3 to 19+1/3th points of the lower (Left and Center below), and that for each grid (Right). Signal derived from the boundary propagating both directions. But it is not diminishing. The free surface height around the boundary is gradually decreasing.

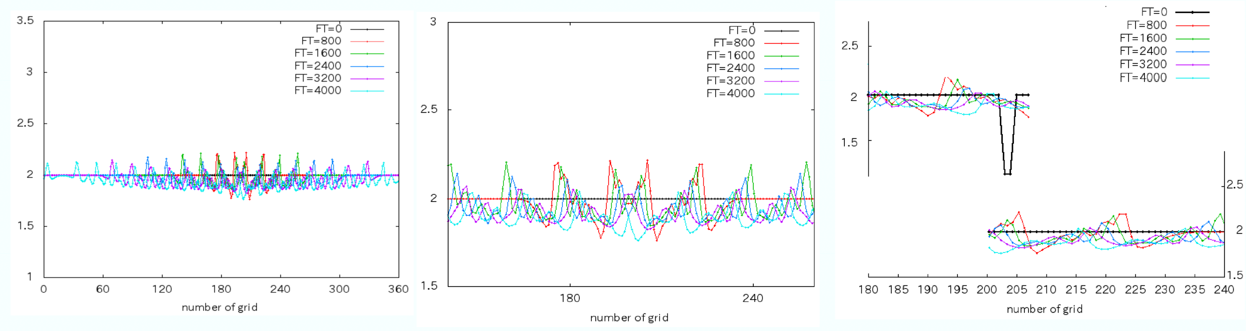

Filter by Shapiro (1971) and modifications in flux estimation and dynamics

Shapiro (1971) proposed the filter below. It diminishes shorter signals (smaller than 4 grid length), but has none to do with longer than that.

$(\partial p_i/\partial t)^t = G_i^t(p^t) \Delta t$,

$G_i^t(p^t) = - (\Delta x / 2)^{16} \delta_{16x} (p^t, i) \Delta t_{ref} / \Delta t$.

Where Δt is time step, Δt_{ref} is reference of it and 10 sec here, Δx is grid size, $\delta_{16x} (p^t, i)$ is the 16th order finite difference analogue of $(\partial^{16}p/\partial x^{16})_i$.

Adding to the filter, it may be useful to modify the flux estimation and dynamics calculation for dumping noise. For instance, $u_{i+1/2}=8M_{i+1/2}/(p_{i-1}+3p_i+3p_{i+1}+p_{i+2})$ instead of $u_{i+1/2}=2M_{i+1/2} /(p_i+ p_{i+1})$, where $M_{i+1/2}$ is momentum at the right interface of i th grid, and $u_{i+1/2}$ is velocity there.

The same figures as above three with Shapiro (1971) and modifications in flux estimation and dynamics. The modification includes 4th order height estimation and 4th order gradient estimation by Levander (1988) in the gravity term, adding to the interface velocity calculation for the flux above.

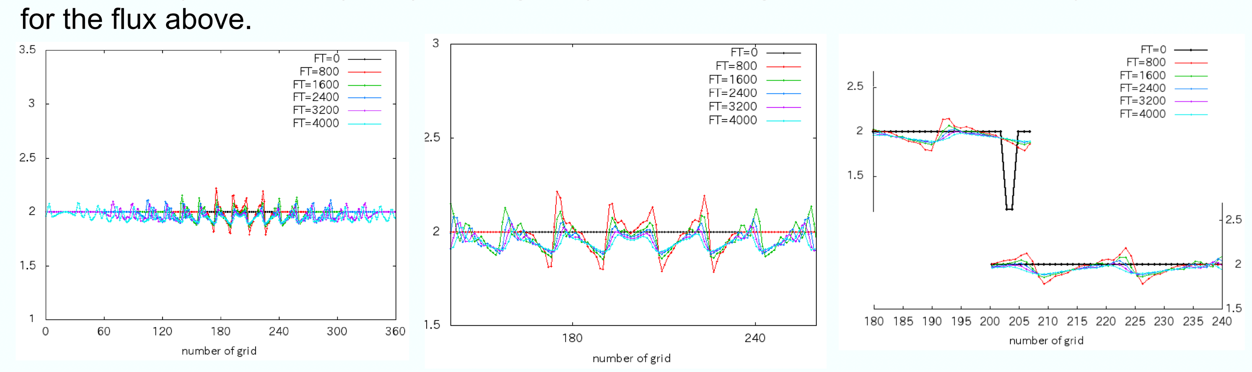

Similar oscillation is propagating for the first 800 steps, but the oscillation seems gradually diminishing in time.

4. Summary

Two types of computational instabilities arising from Yin-Yang boundary are analyzed using one dimensional shallow water model. These are related to

A) influence by a flux adjustment at the boundary,

B) discrepancy in the overlapped area.

As for problem A), we find it difficult to adapt any flux adjustment at the boundary, because imbalance between scalar and momentum field can cause reflection at the boundary. As for problem B), it seems that resonance within the overlapped area is related to the issue. Baba et al. (2010) used Shapiro (1971) discussed here. Although JMA did not use it yet, since Shapiro (1971) requires wider (longer than eight) halo region and larger amount of MPI communication.

References

- Y. Baba, K. Takahashi, and T. Sugimura 2010: Dynamical Core of an Atmospheric General Circulation Model on a Yin-Yang Grid. *Mon. Wea. Rev.*, **138**, 3988-4005.
- W. Hundsdorfer, B. Koren, M. Van Loon, and J. G. Verwer, 1995: A Positive Finite-Difference Advection Scheme. *J. Comp. Phys.* **117**, 35-46.
- Ishida, J., C. Muroi, K. Kawano, and Y. Kitamura 2010: Development of a New Nonhydrostatic Model ASUCA at JMA. *CAS/JSC WGNE Research Activities in Atmospheric and Oceanic Modeling*.
- A. Kageyama and T. Sato 2004: "Yin-Yang grid": An overset grid in spherical geometry. *Geochem. Geophys. Geosys.* **VOL. 5**, Q09005, doi:10.1029/2004GC000734.
- Koren, B, 1993: A robust upwind discretisation method for advection, diffusion and source terms. Numerical Methods for Advection-Diffusion Problems, *Vieweg, Braunschweig*, **117**.
- Levander, A., 1988. Fourth-order finite-difference P-SV seismograms, *Geophysics*, **53**, 1425–1436.
- X. Peng, F. Xiao, and K. Takahashi 2006: Conservative Constraint for a Quasi-Uniform Overset Grid on the Sphere. *Q.J.R. Met. Soc*, **132**, 979-996.
- R. Shapiro 1971: The Use of Linear Filtering as Parameterization of Atmospheric Diffusion. J. Atmospheric Science, 28, 525 – 531.
- T. Sugimura, K. Takahashi, and H. Sakagami 2006: Characteristics of Numerical Error on Overset Grid. *Nagare (in Japanese)*, 25, 247-256.
- D. L. Williamson, J.B. Drake, J.J. Hack, R. Jakob, P.N. Swarztrauber 1992: A Standard Test Set for Numerical Approximations to the Shallow Water Equiations in Spherical Geometry. *J. Comp. Phys*. **102**, 211-224.